

Received January 16, 2020, accepted January 31, 2020, date of publication February 4, 2020, date of current version February 17, 2020.

Digital Object Identifier 10.1109/ACCESS.2020.2971676

Closed Loop Control of Photo Voltaic Emulator Using Fractional Calculus

NASIM ULLAH^{ID1}, FAISAL NISAR^{ID2}, AND AHMAD AZIZ ALAHMADI^{ID1}

¹College of Engineering, Department of Electrical Engineering, Taif University, Ta'if 21974, Saudi Arabia

²Department of Electrical Engineering, CECOS University of IT and Emerging Sciences, Peshawar 25124, Pakistan

Corresponding author: Faisal Nisar (faisal_nisar@yahoo.com)

ABSTRACT Threatening environmental effects have forced the community to utilize green and clean alternative options for the generation of electric power. As a matter of fact, solar energy is a critical source of energy; so the demand for creative research is its peak. However, performing real time experiments on solar PV systems is limited by cost, manufacturing, weather constraints and requirement of large space. Thus an equivalent solar energy photo voltaic (PV) system is required for experimental verification and analysis based on precise simulations. In this research work a PV emulator system based on a buck converter is realized. The main objective of PV Emulator is to replicate the characteristic curves (I-V, P-V) of the real solar panel. In order to compensate the variations in both the load and the parameters of power stage, a robust control system is required. A fractional order sliding mode control scheme (FOSMC) has been designed and investigated in this research work. Results have proved the superior performance of the FOSMC as compared to other classical sliding mode control method. The FOSMC controller and PV emulator are implemented using rapid prototyping technique.

INDEX TERMS Renewable energy, photo voltaic emulator, control system, fractional order control.

I. INTRODUCTION

Rapidly and growing needs for more and clean power sources have forced the community to utilize green and clean alternative options for the future power generation. The utilization factor of the renewable energy sources is expanding exponentially [1]. Amongst wind, hydro, biomass and geothermal sources, solar energy is widely utilized as it is abundant in many parts of the world and it is environment friendly [2].

Knowing about the fact that solar energy is a significant source of energy, the demand for the novel research work plays an important role in attaining the exceptional capacity in generation, integration and utilization of solar power [3]. However to achieve this objective, performing real time experiments on solar PV systems is limited by various factors such as cost of manufacturing, different weather conditions and requirement of large space. Analysis such as capturing of optimal power and minimization of harmonics in the output signals of grid mixing mode of the PV systems require detailed experimental analysis [4]. To sum up the discussion, the above discussed factors impose many limitations in conducting the real time experimentation on solar PV

The associate editor coordinating the review of this manuscript and approving it for publication was Kashif Saleem^{ID}.

systems [5]. For this reason, to reduce human efforts, cost and time consumption, solar PV emulators are introduced, that do not impose time and weather constraints, thus offer a feasible solution for lab testing [6].

The basic idea behind designing a PV emulator is to generate the exact I-V and P-V dynamics as exhibited by the real PV panel. The major challenge behind this design is to reflect the same PV characteristics under varying conditions inclusive of partial shading. Moreover, the emulator output impedance must not vary due to the connectivity of different types of power converters. Thus, the designed PV emulator must be able to interface with power electronic converters, generate exact characteristic curves under partial shading conditions and to compensate the variations in load.

Referring the previous literature, different design methodologies are adopted for developing an effective PV emulator system. The pioneering concept was nurtured by considering a single diode approximation algorithms for testing the power electronics equipment in designing the PV emulator system [7], [8]. Whereas, the approximation technique based on a single diode model shows poor accuracy under variable irradiation effects. To cope with this deficiency, researchers proposed a double diode model approximation, showing robust nature towards changes in irradiation and temperature,

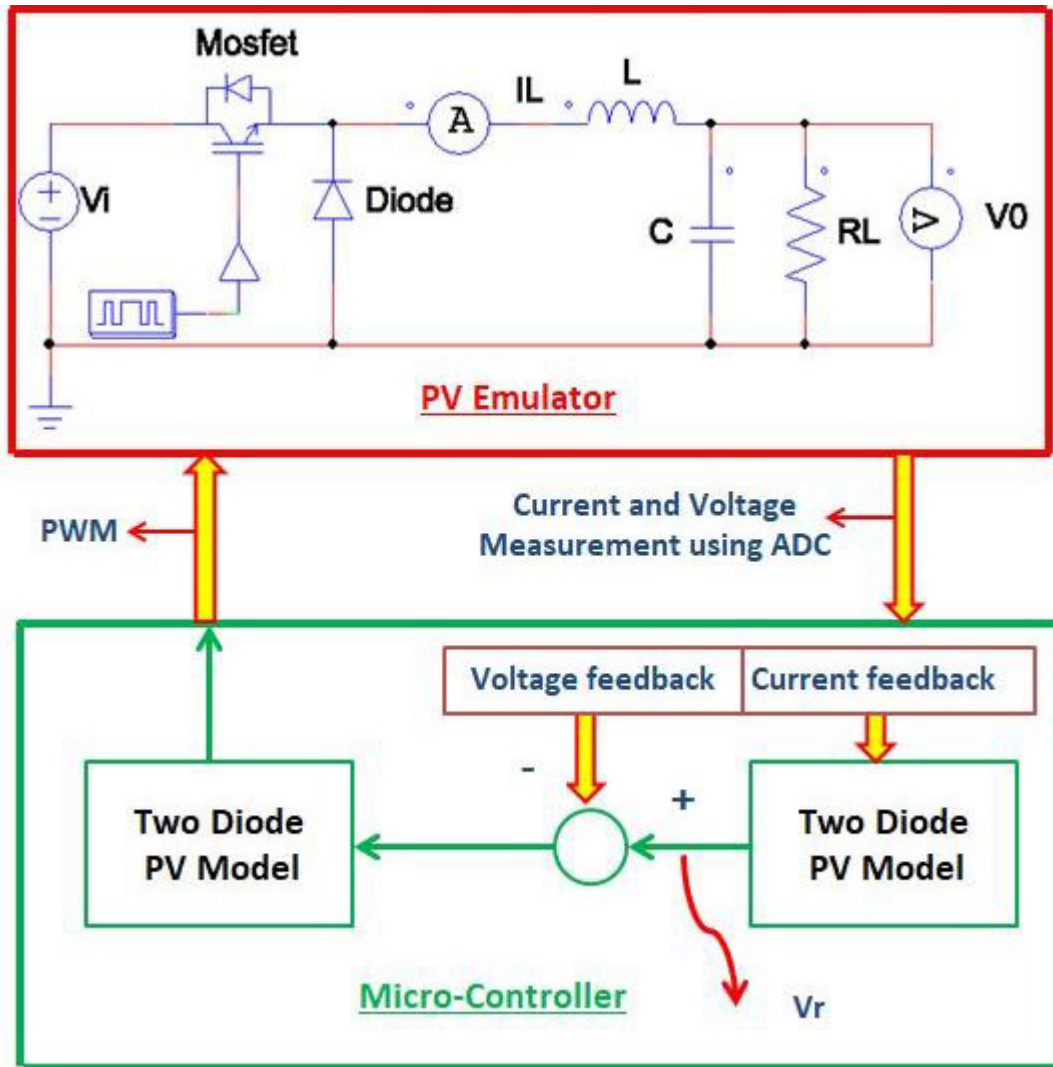


FIGURE 1. Experimental test bench.

resulting in exact I-V and P-V characteristics [9], [10]. However, it lacks the desired degree of robustness against nonlinear load variations and testing of Maximum Power Point Tracking (MPPT) capability. Recently, hardware in the loop PV emulator systems based on power converters have been proposed, being accurate in terms of reliability, efficiency and robustness. Moreover, they also exhibit the ability of MPPT performance testing [11]–[13]. Further, micro-controllers and processors have also been exploited in designing the PV emulator systems [14], [15]. Applications of different real time controllers like Sitara Cortex 9, dspace, FPGA and ARM controllers for PV emulator systems have been reported in literature [16], [17]. However, cost and complexity of PV emulator system rises with the utilization of the above mentioned real time controllers.

Apart from the above cited work, several other techniques have also been reported such as an emulator based on Lambert omega function [18], an emulator based on zero current and voltage switching converter [19], an emulator with battery storage [20], a combined solar and thermo emulator [21],

Internet of Things (IOT) based PV emulator [22] and emulator design methods based on Lab View tools [23]. The main limitation of the above mentioned design attempts is the control system simplicity [19], [24].

As shown in Fig. 1, an important component of PV emulator system is the closed loop control system. Since in the HWIL mode, a power converter is utilized to emulator the I-V and P-V characteristics so the closed loop controller must be robust enough to compensate the parametric variation and disturbances. In [25], an adaptive controller is proposed based on neural network. A method based on resistance comparison and binary search is presented in [26]. Several classical control methods have been reported in the literature such as a classical proportional integral (PI) controller [27], a fuzzy PI control based on pole placement [28], A fuzzy logic based PV emulator [29] and a digitally implemented PI control for PV emulator in [30]. For PV emulator an integer order sliding mode control system is proposed in [31]. All the above mentioned control methods are integer order. Moreover so far most of the literature is focused on the classical PI

control methods and the application of robust control methods to this important emulator is still not very well exploited.

The following are the main contributions of this research work.

1. From the above cited literature, robust control system is rarely exploited for PV emulators. In this article, robust controllers are implemented.

2. As per the authors best knowledge fractional order robust control is never reported for PV emulators.

3. Most of the previous literature is focused on the PV models, while this article is more focused on the closed loop control of PV emulator.

Based on the above literature survey, this article proposes a fractional order robust control method for the PV emulator system. The controller is derived based on the emulator average state space model. The PV emulation system is implemented using HWIL simulation by utilizing the MATLAB/Simulink platforms interfaced with Arduino Due micro-controller board. The rest of the paper is arranged as following. In section II, PV system is modeled, Section III explains the experimental test bench, Section IV shows the controller formulation, Section V discusses the results and finally the Conclusion is derived in Section VI.

II. MODELING OF PV MODULE

The dynamics of PV module are obtained by considering the two diode model [9]. The expression for output current of the module is given by:

$$I_o = I_{PVM} - I_{om1}[e^{-a_1 V_{TM1}} - 1] \quad (1)$$

$$-I_{om2}[e^{-a_2 V_{TM2}} - 1] - \left(\frac{V_M + I_o R_{sm}}{R_{pm}} \right) \quad (2)$$

Current generated by the incident light is denoted by I_{PVM} . The reverse saturation currents of the two diodes are represented by I_{om1} and I_{om2} . The terms V_{TM1} and V_{TM2} are voltages due to thermal activity of the PV module and are given by:

$$V_{TM1,TM2} = \frac{N_{sm} k T}{q} \quad (3)$$

where N_{sm} refers to the number of cells connected in series topology, q is the charge of an electron, k is the Boltzmann's Constant and T is showing the pn junction's temperature measured in kelvin. The diffusion and recombination components of diode current are represented by a_1 and a_2 respectively. The two diode model shows greater accuracy as compared to the single diode model of the PV module. Different parameters appearing in the equation (1,2) can be found as follows:

$$I_{PVM} = (I_{PVM_STC} + K_{im} \Delta T) \frac{G_{2D}}{G_{STC2D}} \quad (4)$$

where I_{PVM_STC} shows the current generated by light at standard test conditions (STCs). K_{im} is the current coefficient of short circuit and is provided by the manufacturer.

Surface irradiance of the cell is give by G_{2D} whereas, irradiance at STCs is give by G_{STC2D} . The reverse saturations currents of diode can be found as:

$$I_{om1}, I_{om2} = \frac{I_{PVM_STC} + K_{im} \Delta T}{e^{(V_{ocm_STC} + K_{vm} \Delta T)/V_{TM}(a_1+a_2)/p} - 1} \quad (5)$$

a_1 is considered unity in accordance to Shockley's theory of diffusion. $a_2 \geq 1.2$ leading to $p \geq 2.2$ as reported in [9].

The values of the two resistors R_{pm} and R_{sm} can be found by an iterative method using the following equation.

$$R_{pm} = \frac{V_{MPT} + I_{MPT} R_{sm}}{I_{PVM} - \frac{V_{MPT}}{P_{Max,E}}} \quad (6)$$

$$+ \frac{V_{MPT} + I_{MPT} R_{sm}}{V_{MPT} + I_{MPT} R_{sm}} \quad (7)$$

$$I_{om1} = \frac{V_{Tm}}{V_{MPT} + I_{MPT} R_{sm}} \quad (8)$$

$$+ \frac{V_{MPT} + I_{MPT} R_{sm}}{V_{MPT} + I_{MPT} R_{sm}} \quad (8)$$

$$I_{om2} = \frac{V_{Tm}(p-1)}{V_{Tm}(p-1) - 2} \quad (8)$$

The iteration process is started by choosing the value of R_{sm} zero and R_{pm} is chosen using the following relation.

$$R_{pm0} = \frac{V_{MPT}}{I_{scn} - I_{MPT}} - \frac{V_{ocn} - V_{MPT}}{I_{MPT}} \quad (9)$$

The two terms appearing in the expression for R_{pm0} are the slopes of the line segments related to short circuit current and open circuit voltage at maximum power point respectively.

III. EXPERIMENTAL TEST BENCH

The experimental test bench is shown in Fig. 1. A two diode PV model is implemented on Arduino micro-controller. There are two types of inputs to the PV model. The first input consists of the environmental parameters such as temperature and irradiance. The second input is the feedback current that is measured at the output of the buck converter. The PV model outputs the reference voltage which is used as a command signal for the voltage loop of the PV emulator. As shown in Fig. 1, the measured voltage feedback signal is read through analog to digital converter (ADC1) pin of the micro-controller and a closed loop voltage control loop is implemented. The control system generates appropriate PWM signal to drive the buck converter used as PV emulator. The experiment is run in the hardware in the loop (HWIL) mode. As a first step the PV model and the control blocks are implemented in MATLAB/Simulink. Then by using real time workshop and embedded coders, the model is compiled into code and the output or hex file is programmed to the RAM of the target micro-controller. The model is run in external mode so the measured data at the output of PV emulator is read back in Simulink environment. Software low pass filters are applied to the data to remove unwanted noise from the measured signals.

IV. CONTROLLER FORMULATION

In this section a fractional order proportional integral Control (FOPI) is introduced for the voltage control loop of the PV emulator system. Before discussing the control law, fractional calculus is introduced briefly.

Definition 1: The Riemann–Liouville fractional order integration and derivative of a function $f(t)$ are expressed as shown in Eq. 10 and Eq. 11 [32], [33].

$${}_{t_0}I_t^\alpha f(t) = D_t^{-\alpha}f(t) = \frac{1}{\Gamma(\alpha)} \int_{t_0}^t \frac{f(\tau)}{(t-\tau)^{1-\alpha}} d\tau \quad (10)$$

$${}_{t_0}D_t^\alpha f(t) = \frac{d^\alpha}{dt^\alpha} f(t) = \frac{1}{\Gamma(m-\alpha)} \frac{d^m}{dt^m} \int_{t_0}^t \frac{f(\tau)}{(t-\tau)^{\alpha-m+1}} d\tau \quad (11)$$

Here $\Gamma(\cdot)$ represents the gamma function,, $m \in N$ and $m - 1 < \alpha \leq m$

From Eq. 10 and Eq. 11 the following relation holds:

$${}_{t_0}D_t^\alpha ({}_{t_0}I_t^\alpha f(t)) = f(t)$$

Definition 2: The Caputo fractional order derivative of a function $f(t)$ is given by [32], [33].

$$\begin{aligned} {}_{t_0}D_t^\alpha f(t) \\ = \begin{cases} \frac{1}{\Gamma(m-\alpha)} \int_{t_0}^t \frac{f^{(m)}(\tau)}{(t-\tau)^{\alpha-m+1}} d\tau; & m-1 < \alpha < m \\ \frac{d^m}{dt^m} f(t); & \alpha = m \end{cases} \end{aligned} \quad (12)$$

Rieman-Liouville and Caputo definitions are very much similar; the only difference lies in dealing with the initial conditions. In Rieman-Liouville definition, the initial conditions are non-integer while for Caputo definition they are of integer order.

The average state space model of the buck converter is derived as following:

$$\begin{aligned} \frac{dI_L}{dt} &= \frac{uV_i}{L} - \frac{V_0}{L} + d_i \\ \frac{dV_0}{dt} &= \frac{I_L}{C} - \frac{V_0}{R_L C} + d_v \end{aligned} \quad (13)$$

Here d_i and d_v represent the disturbance introduced in the system's model due to the uncertainty in the power stage parameters and load. d_i and d_v are represented as following.

$$\begin{aligned} d_v &= \frac{uV_i}{\Delta L} - \frac{V_0}{\Delta L} \\ d_i &= \frac{I_L}{\Delta C} - \frac{V_0}{\Delta R_L \Delta C} \end{aligned} \quad (14)$$

The parametric uncertainty in Eq. 14 represents the variation in the power stage parameters i.e. L and C . These variations may occur over time due to aging effect when a converter is operating over a long time span. Secondly the drift in the parameters can be due to the temperature effects etc. Apart from the power stage parametric uncertainties, the load R_L connected at the output of the buck converter is

taken as variable in this particular case. A fractional order voltage sliding surface S_V is defined as following:

$$S_V = c_1 D^{-\alpha} (V_r - V_0) + c_2 \int (\dot{V}_r - \dot{V}_0) \quad (15)$$

In Eq. 14, c_1, c_2 are the constants, V_r represents the reference voltage command and V_0 is the output voltage. By taking the first derivative on both sides of Eq. 15, one obtains the following expression.

$$\dot{S}_V = c_1 D^{1-\alpha} e_V + c_2 \dot{e}_V \quad (16)$$

Here the voltage error is represented as $e_V = V_r - V_0$, while its first derivative is expressed as $\dot{e}_V = \dot{V}_r - \dot{V}_0$. Expanding Eq. 16 in term of the capacitor voltage dynamics, the resultant expression is given by Eq. 17.

$$\dot{S}_V = c_1 D^{1-\alpha} e_V + c_2 \dot{V}_r - c_2 \frac{I_L}{C} + c_2 \frac{V_0}{R_L C} - c_2 d_v \quad (17)$$

Using Eq. 17, choose the reference current command shown in Eq. 18.

$$I_{L-ref} = C \left\{ \frac{V_0}{R_L C} + \dot{V}_r + \frac{c_1}{c_2} D^{1-\alpha} e_V + \frac{K_1}{c_2} S_V \right\} \quad (18)$$

A current sliding surface S_I is defined as

$$S_I = c_3 D^{-\alpha} (I_{L-ref} - I_L) + c_4 \int (\dot{I}_{L-ref} - \dot{I}_L) \quad (19)$$

In Eq. 19, c_3, c_4 are the constants, I_{L-ref} represents the reference current command and I_L is the inductor current. By taking the first derivative on both sides of Eq. 19, one obtains the following expression

$$\dot{S}_I = c_3 D^{1-\alpha} e_I + c_4 \dot{e}_I \quad (20)$$

Here the current error is represented as $e_I = I_{L-ref} - I_L$, while its first derivative is expressed as $\dot{e}_I = \dot{I}_{L-ref} - \dot{I}_L$. Expanding Eq. 20 in term of the inductor current dynamics, the resultant expression is given by Eq. 21.

$$\dot{S}_I = c_3 D^{1-\alpha} e_I + c_4 \dot{I}_{L-ref} - c_4 \frac{uV_i}{L} + c_4 \frac{V_0}{L} - c_4 d_i \quad (21)$$

The current control law is derived as

$$\begin{aligned} u &= u_{eq} + u_s \\ u_{eq} &= \frac{L}{V_i} \left\{ \frac{c_3}{c_4} D^{1-\alpha} e_I + \frac{V_0}{L} + \dot{I}_{L-ref} + K_2 S_I \right\} \\ u_s &= \frac{L}{V_i} \left\{ \frac{K_3}{c_4} \text{sgn}(S_I) \right\} \end{aligned} \quad (22)$$

In Eq. 19 and 22, K_2 and K_3 represent the control system constants.

To prove the stability of the closed loop, the Lyapunov function is expressed as given in Eq. 23.

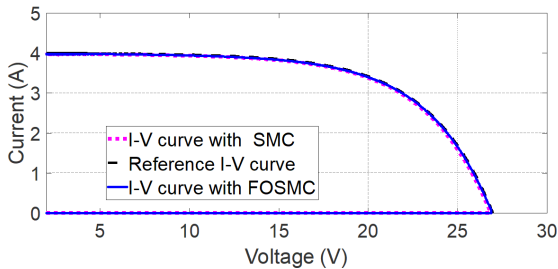
$$V = \frac{1}{2} S_V^2 + \frac{1}{2} S_I^2 \quad (23)$$

Taking the first derivative of Eq. 23 and combining it with Eq. 17, 18 and Eq. 21, 22 yields the following expression.

$$\dot{V} = -K_1 S_V^2 - K_2 S_I^2 - K_3 |S_I| + c_2 d_v + c_4 d_i \quad (24)$$

TABLE 1. PV emulator and controller parameters.

Emulator Parameters	Value	Control Parameter	Value
L	10 μH	c_1	1.5
C	22 mF	c_2	0.5
R	10 ohms	c_3	1.2
f_s	32Khz	c_4	2.5
P_{pv}	26V, 3.96A	K_1	1.5
P_r	100 watts	K_2	0.5
V_i	30 V	K_3	2.5
V_0	(26-0) V	α	.95

**FIGURE 2.** I-V curve of emulator at $T = 25 C^\circ$ and $I = 1000 W.m^{-2}$.

Assuming that the upper bounds of d_v and d_i are known, then by letting K_1 , K_2 and K_3 such that the accumulative value of the terms $-(K_1S_V^2 + K_2S_I^2 + K_3|S_I|)$ is always greater than $(c_2d_v + c_4d_i)$ so that $\dot{V} < 0$.

V. EXPERIMENTAL RESULTS AND DISCUSSION

The PV emulator is tested on a 100 watts power converter module. The maximum open circuit voltage $V_0 = 26 V$ and $I_{sc} = 3.98 A$ at standard operating conditions. The parameters of the control system are tabulated in table 1. The performance of the PV emulator with proposed control is compared with a classical sliding mode (SMC) control system. The derivation of classical SMC control is presented in Appendix A. The switching control u_s of the proposed and classical SMC control schemes shown in Eq. 22 and 32 are approximated by a smooth saturation function. As a load device a buck converter is connected at the output of the PV emulator. The experimental results are collected in HWIL simulation and the following two cases are discussed.

A. CASE 1: PV EMULATOR UNDER IDEAL CONDITIONS

In this section it is assumed that the disturbance terms and power stage parametric variations in the PV emulator is zero. $I - V$ and $P - V$ curves of the PV emulators are plotted under the proposed control scheme for different operating conditions. The obtained results are compared with the results obtained for PV emulator system with classical SMC based control system.

Fig. 2 and 3 show the $I - V$ curve of the emulator under ideal conditions with the action of proposed control and the classical SMC. The experiment is conducted at a temperature of $25C^\circ$ and the irradiance, $I = 1000 W.m^{-2}$. From Fig. 2 it is evident that the maximum current of 3.96 A is emulated and the system perfectly acts as a constant current source. In order to have a fair comparison between the proposed control and the classical SMC control, Fig. 3 shows the zoom version of

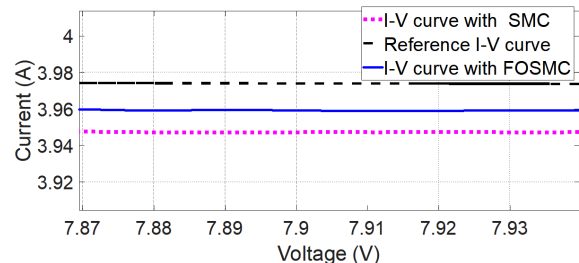
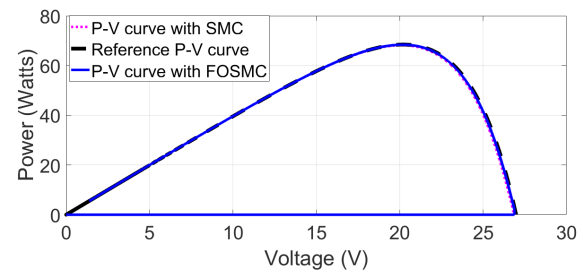
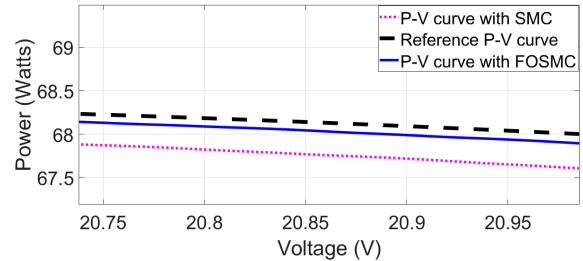
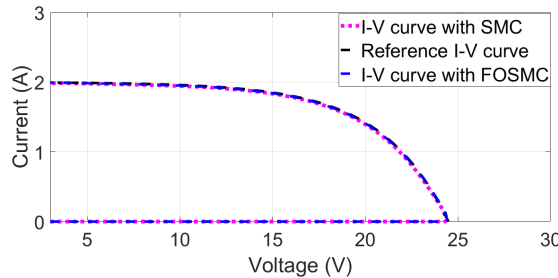
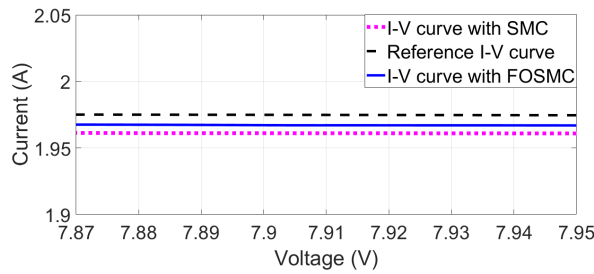
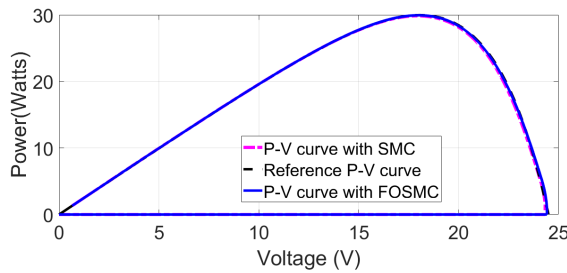
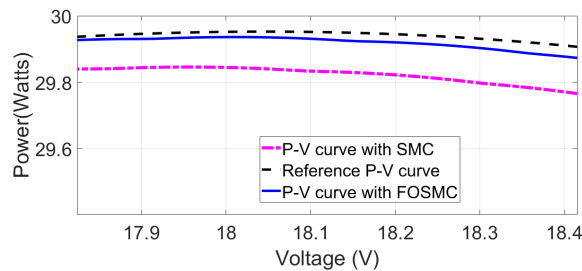
**FIGURE 3.** Zoom view of I-V curve@t $T = 25 C^\circ$ and $I = 1000 W.m^{-2}$.**FIGURE 4.** P-V curve of emulator at $T = 25 C^\circ$ and $I = 1000 W.m^{-2}$.**FIGURE 5.** Zoom view of P-V curve@t $T = 25 C^\circ$ and $I = 1000 W.m^{-2}$.

Fig. 2. From Fig. 3 it is concluded that the PV emulator with proposed control system, closely matches the behaviour of the actual PV model while with SMC control, the error in the $I - V$ curve is almost doubled.

Fig. 4 and 5 show the $P - V$ curve of the emulator under ideal conditions with the action of proposed control and the classical SMC. The experiment is conducted at a temperature of $25C^\circ$ and the irradiance $I = 1000 W.m^{-2}$. From Fig. 4 it is evident that the maximum point is emulated with voltage $V = 21$ volts and the system perfectly tracks the reference $P - V$ curve. The zoom version of the $P - V$ curve is shown in Fig. 5. From the obtained results it is confirmed that under the proposed control scheme, the emulator's $P - V$ response closely matches with the reference curve, while with classical SMC, the deviation is more.

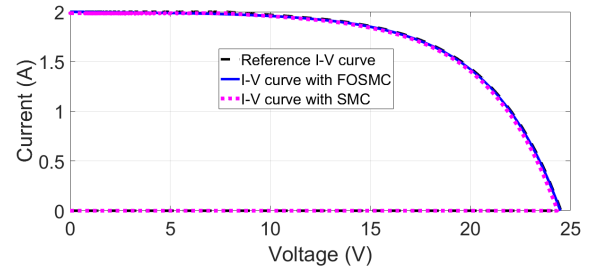
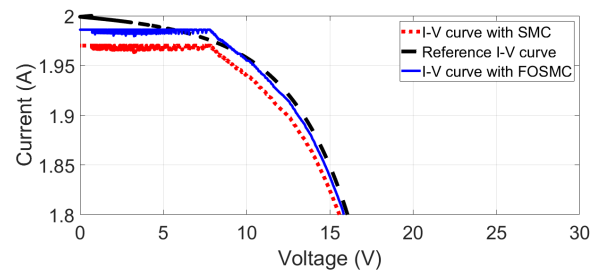
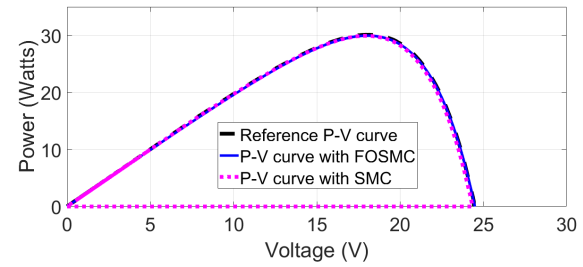
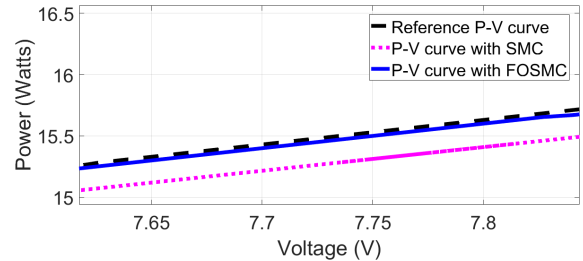
Fig. 6 and 7 show the $I - V$ curve of the emulator under ideal conditions with the action of proposed control and the classical SMC. The experiment is conducted at a temperature of $25C^\circ$ and the irradiance $I = 400 W.m^{-2}$. From the obtained results it is recorded that by decreasing the irradiance by 60 percent, both the current and voltage also reduces. The current is reduced to 1.98A and the output voltage reduces to 24.9 volts. The results presented

FIGURE 6. I-V curve of emulator at $T = 25\text{ C}^\circ$ and $I = 400\text{ W.m}^{-2}$.FIGURE 7. Zoom view of I-V curve@ $t = 25\text{ C}^\circ$ and $I = 400\text{ W.m}^{-2}$.FIGURE 8. P-V curve of emulator at $T = 25\text{ C}^\circ$ and $I = 400\text{ W.m}^{-2}$.FIGURE 9. Zoom view of P-V curve@ $t = 25\text{ C}^\circ$ and $I = 400\text{ W.m}^{-2}$.

in Fig. 7 confirms the superior performance of the PV emulator with the proposed control. Similarly Fig. 8 and 9 show the P-V curve of the emulator. It is noted from Fig. 8 that with the reduced value of the irradiance, the peak power also reduces and the recorded value is around 30 watts. From the results presented in Fig. 9, it is evident that the emulator tracks the reference PV curve with FOSMC control perfectly, while the deviations in case of classical SMC are more as compared with the proposed control method.

B. CASE 2: PV EMULATOR UNDER POWER STAGE PARAMETER VARIATIONS

In this section the effect of power stage parametric variations is included in the experiment. $I - V$ and $P - V$ curves of

FIGURE 10. I-V curve of emulator at $T = 25\text{ C}^\circ$ and $I = 400\text{ W.m}^{-2}$.FIGURE 11. Zoom view of I-V curve@ $t = 25\text{ C}^\circ$ and $I = 400\text{ W.m}^{-2}$.FIGURE 12. P-V curve of emulator at $T = 25\text{ C}^\circ$ and $I = 400\text{ W.m}^{-2}$.FIGURE 13. Zoom view of P-V curve@ $t = 25\text{ C}^\circ$ and $I = 400\text{ W.m}^{-2}$.

the PV emulators are plotted under the proposed control scheme. A total variation of 20% in power stage parameters is subjected with $L \pm 20\%$ and $C \pm 20\%$.

Fig. 10 and 11 show the I-V curve recorded from the PV emulator with parameter variation. In the I-V curve, the parameters variation is introduced at a voltage $V = 7.6$ volts and current $I = 1.97$ A. The zoom version of the emulator's I-V response is shown in Fig. 11. From the presented results, it is confirmed that under the action of the proposed control scheme, the emulator's I-V curve closely resembles the reference curve, while in case of classical SMC, the deviation from the reference curve is more.

Similarly Fig. 12 and 13 confirms the superior performance of the PV emulator under the action of the proposed control scheme.

VI. CONCLUSION

This work is focused on the robust behavior of the closed loop control system for a PV emulator. Two variants of controllers are analyzed. The first controller was derived based on the concepts of the variable structure control and fractional calculus. For a fair comparison, a classical SMC control system was also tested. From the presented results, the superiority of the proposed FOSMC control system is confirmed. In comparison to the classical SMC control method, the PV emulator exhibited less deviation from the ideal I-V and P-V curves under the action of the proposed control scheme.

APPENDIX

A classical sliding surface S_V is defined as following:

$$S_V = c_1(V_r - V_0) + c_2 \int (V_r - V_0) \quad (25)$$

In Eq. 25, all the constants are defined in Section IV. By taking the first derivative on both sides of Eq. 25, one obtains the following expression.

$$\dot{S}_V = c_1 \dot{e}_V + c_2 e_V \quad (26)$$

Expanding Eq. 26 in term of the capacitor voltage dynamics, the resultant expression is given by Eq. 27.

$$\dot{S}_V = c_2 e_V + c_1 \dot{V}_r - c_1 \frac{I_L}{C} + c_1 \frac{V_0}{R_L C} - c_1 d_V \quad (27)$$

Using Eq. 27, choose the reference current command shown in Eq. 28.

$$I_{L-ref} = C \left\{ \frac{V_0}{R_L C} + \dot{V}_r + \frac{c_2}{c_1} e_V + \frac{K_1}{c_1} S_V \right\} \quad (28)$$

A current sliding surface S_I is defined as

$$S_I = c_3(I_{L-ref} - I_L) + c_4 \int (I_{L-ref} - I_L) \quad (29)$$

All the constants of Eq. 29 are defined in previous section. By taking the first derivative on both sides of Eq. 29, one obtains the following expression

$$\dot{S}_I = c_3 \dot{e}_I + c_4 e_I \quad (30)$$

Expanding Eq. 30 in term of the inductor current dynamics, the resultant expression is given by Eq. 31.

$$\dot{S}_I = c_4 e_I + c_3 \dot{I}_{L-ref} - c_3 \frac{uV_i}{L} + c_3 \frac{V_0}{L} - c_3 d_i \quad (31)$$

The current control law is derived as

$$\begin{aligned} u &= u_{eq} + u_s \\ u_{eq} &= \frac{L}{V_i} \left\{ \frac{c_4}{c_3} e_I + \frac{V_0}{L} + \dot{I}_{L-ref} + \frac{K_2}{c_3} S_I \right\} \\ u_s &= \frac{L}{V_i} \left\{ \frac{K_3}{c_3} \operatorname{sgn}(S_I) \right\} \end{aligned} \quad (32)$$

To prove the stability of the closed loop, the Lyapunov function is expressed as given in Eq. 33.

$$V = \frac{1}{2} S_V^2 + \frac{1}{2} S_I^2 \quad (33)$$

Taking the first derivative of Eq. 33 and combining it with Eq. 27, 28 and Eq. 31, 32 yields the following expression.

$$\dot{V} = -K_1 S_V^2 - K_2 S_I^2 - K_3 |S_I| + c_2 d_V + c_4 d_i \quad (34)$$

Assuming that the upper bounds of d_V and d_i are known, then by letting K_1, K_2 and K_3 such that the accumulative value of the terms $-(K_1 S_V^2 + K_2 S_I^2 + K_3 |S_I|)$ is always greater than $(c_2 d_V + c_4 d_i)$ so that $\dot{V} < 0$

REFERENCES

- [1] J. P. Ram, H. Manghani, D. S. Pillai, T. S. Babu, M. Miyatake, and N. Rajasekar, "Analysis on solar PV emulators: A review," *Renew. Sustain. Energy Rev.*, vol. 81, pp. 149–160, Jan. 2018.
- [2] T. Sudhakar Babu, J. Prasanth Ram, K. Sangeetha, A. Laudani, and N. Rajasekar, "Parameter extraction of two diode solar PV model using Fireworks algorithm," *Solar Energy*, vol. 140, pp. 265–276, Dec. 2016.
- [3] J. P. Ram, T. S. Babu, T. Dragicevic, and N. Rajasekar, "A new hybrid bee pollinator flower pollination algorithm for solar PV parameter estimation," *Energy Convers. Manage.*, vol. 135, pp. 463–476, Mar. 2017.
- [4] C. S. Solanki, *Solar Photovoltaics: Fundamentals, Technologies and Applications*. New Delhi, India: PHI Learning, 2015.
- [5] J. P. Ram, T. S. Babu, and N. Rajasekar, "A comprehensive review on solar PV maximum power point tracking techniques," *Renew. Sustain. Energy Rev.*, vol. 67, pp. 826–847, Jan. 2017.
- [6] P. E. Marenholtz, "Programmable solar array simulator," *IEEE Trans. Aerosp. Electron. Syst.*, vol. AES-2, no. 6, pp. 104–107, Nov. 1966.
- [7] H. Nagayoshi, S. Orio, Y. Kono, and H. Nakajima, "Novel PV array/module I-V curve simulator circuit," in *Proc. Conf. Rec. 29th IEEE Photovoltaic Spec. Conf.*, Oct. 2003, pp. 1535–1538.
- [8] O.-M. Midtgard, "A simple photovoltaic simulator for testing of power electronics," in *Proc. Eur. Conf. Power Electron. Appl.*, 2007, pp. 1–10.
- [9] K. Ishaque, Z. Salam, and Syafaruddin, "A comprehensive MATLAB Simulink PV system simulator with partial shading capability based on two-diode model," *Solar Energy*, vol. 85, no. 9, pp. 2217–2227, Sep. 2011.
- [10] A. Sanaullah and H. A. Khan, "Design and implementation of a low cost Solar Panel emulator," in *Proc. IEEE 42nd Photovoltaic Spec. Conf. (PVSC)*, Jun. 2015, pp. 1–5.
- [11] S. N. Deshkar, S. B. Dhale, J. S. Mukherjee, T. S. Babu, and N. Rajasekar, "Solar PV array reconfiguration under partial shading conditions for maximum power extraction using genetic algorithm," *Renew. Sustain. Energy Rev.*, vol. 43, pp. 102–110, Mar. 2015.
- [12] J. Prasanth Ram and N. Rajasekar, "A novel flower pollination based global maximum power point method for solar maximum power point tracking," *IEEE Trans. Power Electron.*, vol. 32, no. 11, pp. 8486–8499, Nov. 2017.
- [13] J. Ram, N. Rajasekar, and M. Miyatake, "Design and overview of maximum power point tracking techniques in wind and solar photovoltaic systems: A review," *Renew. Sustain. Energy Rev.*, vol. 73, pp. 1138–1159, Jun. 2017.
- [14] S. M. Azharuddin, M. Vysakh, H. V. Thakur, B. Nishant, T. S. Babu, K. Muralidhar, D. Paul, B. Jacob, K. Balasubramanian, and N. Rajasekar, "A near accurate solar PV emulator using dSPACE controller for real-time control," *Energy Procedia*, vol. 61, pp. 2640–2648, 2014.
- [15] C.-C. Chen, H.-C. Chang, C.-C. Kuo, and C.-C. Lin, "Programmable energy source emulator for photovoltaic panels considering partial shadow effect," *Energy*, vol. 54, pp. 174–183, Jun. 2013.
- [16] G. Tornez-Xavier, F. Gomez-Castaneda, J. Moreno-Cadenas, and L. Flores-Navia, "FPGA development and implementation of a solar panel emulator," in *Proc. 10th Int. Conf. Electr. Eng., Comput. Sci. Autom. Control (CCE)*, Sep. 2013, pp. 467–472.
- [17] A. C. Atoche, J. V. Castillo, J. Ortegón-Aguilar, R. Carrasco-Alvarez, J. S. Gó, and A. Colli-Menchí, "A high-accuracy photovoltaic emulator system using ARM processors," *Solar Energy*, vol. 120, pp. 389–398, Oct. 2015.

- [18] T. Jiang, G. Putrus, S. McDonald, M. Conti, B. Li, and D. Johnston, “Generic photovoltaic system emulator based on lambert omega function,” in *Proc. 46th Int. Universities’ Power Eng. Conf. (UPEC)*, 2011, pp. 1–5.
- [19] Z. Zhuo, J. Zhang, H. Sun, G. Wang, X. Hu, and S. Zhao, “Research on photovoltaic array emulator system based on a novel zero-voltage zero-current switching converter,” in *Proc. Asia-Pacific Power Energy Eng. Conf.*, 2010, pp. 1–4.
- [20] A. Mukerjee and N. Dasgupta, “DC power supply used as photovoltaic simulator for testing MPPT algorithms,” *Renew. Energy*, vol. 32, no. 4, pp. 587–592, Apr. 2007.
- [21] P. Calò, G. Fiscelli, F. Lo Bue, A. Di Stefano, and G. Giaconia, “An electronic emulator of combined photovoltaic and solar thermal systems,” in *Proc. EVER*, 2010, pp. 1–5.
- [22] E. Golubovic, A. Sabanovic, and B. C. Ustundag, “Internet of Things inspired photovoltaic emulator design for smart grid applications,” in *Proc. 3rd Int. Istanbul Smart Grid Congr. Fair (ICSG)*, Apr. 2015, pp. 1–6.
- [23] D. S. L. Dolan, J. Durago, and Taufik, “Development of a photovoltaic panel emulator using Labview,” in *Proc. 37th IEEE Photovoltaic Spec. Conf.*, Jun. 2011, pp. 1795–1800.
- [24] J. Agrawal and M. Aware, “Photovoltaic system emulator,” in *Proc. IEEE Int. Conf. Power Electron., Drives Energy Syst. (PEDES)*, Dec. 2012, pp. 1–6.
- [25] R. Ayop and C. Wei Tan, “An adaptive controller for photovoltaic emulator using artificial neural network,” *Indonesian J. Elect. Eng. Comput. Sci.*, vol. 5, no. 3, pp. 556–563, May 2017.
- [26] R. Ayop and C. W. Tan, “Improved control strategy for photovoltaic emulator using resistance comparison method and binary search method,” *Solar Energy*, vol. 153, pp. 83–95, Sep. 2017.
- [27] I. Moussa, A. Khedher, and A. Bouallegue, “Design of a low-cost PV emulator applied for PVECS,” *Electronics*, vol. 8, no. 2, p. 232, Feb. 2019.
- [28] M. C. Di Piazza, M. Pucci, A. Ragusa, and G. Vitale, “A grid-connected system based on a real time PV emulator: Design and experimental set-up,” in *Proc. 36th Annu. Conf. IEEE Ind. Electron. Soc. (IECON)*, Nov. 2010, pp. 3237–3243.
- [29] R. Ayop, “Control of the photovoltaic emulator using fuzzy logic based resistance feedback and binary search,” Ph.D. dissertation, School Elect. Eng. Fac. Eng., Universiti Teknologi Malaysia, Johor Bahru, Malaysia, 2018.
- [30] J. Zhao and J. W. Kimball, “A digitally implemented photovoltaic simulator with a double current mode controller,” in *Proc. 27th Annu. IEEE Appl. Power Electron. Conf. Expo. (APEC)*, Feb. 2012, pp. 53–58.
- [31] A. Cordeiro, D. Foito, and V. Fernao Pires, “A PV panel simulator based on a two quadrant DC/DC power converter with a sliding mode controller,” in *Proc. Int. Conf. Renew. Energy Res. Appl. (ICRERA)*, Nov. 2015, pp. 928–932.
- [32] N. Ullah, W. Shaoping, M. I. Khattak, and M. Shafi, “Fractional order adaptive fuzzy sliding mode controller for a position servo system subjected to aerodynamic loading and nonlinearities,” *Aerospace Sci. Technol.*, vol. 43, pp. 381–387, Jun. 2015.
- [33] N. Ullah, S. Han, and M. Khattak, “Adaptive fuzzy fractional-order sliding mode controller for a class of dynamical systems with uncertainty,” *Trans. Inst. Meas. Control*, vol. 38, no. 4, pp. 402–413, 2016.



NASIM ULLAH received the Ph.D. degree in mechatronics engineering from Beihang University, Beijing, China, in 2013. From 2006 to 2010, he was a Senior Design Engineer with IICS, Pakistan. He is currently an Associate Professor of electrical engineering with Taif University, Saudi Arabia. His research interests include renewable energy, flight control systems, integer and fractional order modeling of dynamic systems, integer/fractional order adaptive robust control methods, fuzzy/NN, hydraulic and electrical servos, epidemic, and vaccination control strategies.



FAISAL NISAR received the M.S. degree in electrical engineering from the CECOS University of IT and Emerging Sciences, Peshawar, in 2019. His research interests include PV emulation, control systems, and estimation theory.



AHMAD AZIZ ALAHMADI received the Ph.D. degree in nano-electronic devices from the School of Engineering, Ohio University, OH, USA. He is currently an Associate Professor with the Department of Electrical Engineering, Faculty of Engineering, Taif University, Saudi Arabia. Since July 2017, he has been the Vice-Dean of the Faculty of Engineering with Taif University. His research interests include control systems and nano-electronic devices.

• • •